Submitted to the
International Europhysics Conference on High Energy Physics
July 17 - 23, 2003, Aachen, Germany

Abstract: 518 **Session: HP**

Substructure dependence of jet cross sections at HERA

ZEUS Collaboration

Abstract

Differential cross sections for jets produced in the photoproduction regime have been measured with the ZEUS detector at HERA using an integrated luminosity of 82 pb^{-1}. Jets were identified using the k_T-cluster algorithm in the longitudinally invariant inclusive mode. Measurements of differential cross sections are presented for jets characterised by their substructure as a function of the jet variables to study the underlying color dynamics. Leading-logarithm parton-shower Monte Carlo calculations were compared to the results and used to disentangle the contributing two-body hard-scattering subprocesses.

1 Introduction

Photoproduction at HERA is studied by means of ep scattering at low four-momentum transfers ($Q^2 \approx 0$, where Q^2 is the virtuality of the exchanged photon). In photon-proton reactions, two types of QCD processes contribute to jet production at leading order (LO) [1, 2]: either the photon interacts directly with a parton in the proton (the direct process) or the photon acts as a source of partons which scatter off those in the proton (the resolved process). The dominant partonic subprocesses responsible for jet production in the kinematic region presented in this paper are $\gamma g \to q\bar{q}$ and $q_\gamma g_p \to qg$. The kinematics of these two-to-two subprocesses are such that the majority of the jets in the region of jet pseudorapidity $\eta^{\text{jet}} < 0$ (incoming positron direction) are predicted to originate from outgoing quarks while the fraction of gluon-initiated jets increases as η^{jet} increases [3]. Therefore, the experimental investigation of the jet properties as a function of the jet pseudorapidity allows the study of the characteristics of quark- and gluon-initiated jets [4].

The distribution of the angle between the jet-jet axis and the beam direction in the dijet centre-of-mass system ($\cos\theta^*$) reflects the underlying parton dynamics and is sensitive to the spin of the exchanged particle. In the case of direct-photon interactions, the contributing subprocesses at LO QCD are (i) $\gamma q(\bar{q}) \to gq(\bar{q})$ and (ii) $\gamma g \to q\bar{q}$, which involve quark exchange in the s, t and u channels. The matrix element squared for subprocess (i) is proportional to $[(-\hat{u})/\hat{s} + \hat{s}/(-\hat{u})]$, where $(\hat{s}, \hat{t}, \hat{u})$ are the Mandelstam variables for the two-body hard process. The matrix element for (ii) is obtained by crossing $\hat{s} \leftrightarrow \hat{t}$. The behaviour of the dijet angular distribution as $|\cos\theta^*| \to 1$ is the same for all subprocesses and proportional to $(1 - |\cos\theta^*|)^{-1}$. In the case of resolved-photon interactions, the contributing subprocesses are the same as for dijet production in $p\bar{p}$ collisions ($qg \to qg$, $qq' \to qq'$, $gg \to gg$, ...). The dominant subprocesses are those that involve gluon exchange and the behaviour of the dijet angular distribution is proportional to $(1-|\cos\theta^*|)^{-2}$ as $|\cos\theta^*| \to 1$. The different behaviour of the dijet angular distribution for resolved and direct processes has been measured in photoproduction at HERA [5]. The study of the angular distribution for dijet events with quarks and/or gluons in the final state, provides also a handle to investigate the underlying parton dynamics [4].

The internal structure of a jet is expected to depend mainly on the type of primary parton, quark or gluon, from which it originated and to a lesser extent on the particular hard scattering process and can be studied using the jet shape [6] and the subjet multiplicity [7]. At sufficiently high jet transverse energy, where fragmentation effects become negligible, the jet shape and subjet multiplicity are expected to be calculable in perturbative QCD.

Perturbative QCD predicts that gluon-initiated jets are broader than quark-initiated jets due to the larger colour charge of the gluon. At HERA, measurements have been pre-

sented of jet shapes using an iterative cone algorithm [3] and of jet shapes and mean subjet multiplicities using the k_T-cluster algorithm [8] in photoproduction. The jets were observed to become broader and the mean subjet multiplicity to increase as $\eta^{\rm jet}$ increases, in agreement with the predicted increase in the fraction of final-state gluon-initiated jets. Jet shapes and subjet multiplicities can then be used to study the internal structure of the jets and classify them: a "thick"-jet sample would be expected to be enriched in gluon-initiated jets, whereas a "thin"-jet sample would be enriched in quark-initiated jets. Thus, the measurement of the $\eta^{\rm jet}$ dependence of the jet cross sections for "thick"- and "thin"-jet samples would allow the contributing two-body hard-scattering subprocesses to be disentangled.

In this paper, measurements of differential inclusive jet cross sections as a function of $\eta^{\rm jet}$ and $E_T^{\rm jet}$ for samples of jets separated according to their shape and subjet multiplicity are presented. This analysis benefits from a data sample which represents a 2-fold increase with respect to the previous measurements [4], and from the use of simultaneous cuts on the jet shape and subjet multiplicity, which produces purer samples of quark- and gluon-initiated jets. Furthermore, inclusive jet cross sections present several theoretical advantages with respect to dijet cross sections in a QCD analysis: the inclusive jet cross sections are infrared insensitive, are better suited to test resummed calculations and the theoretical uncertainties are smaller than for dijet cross sections. Measurements of differential dijet cross sections as a function of $\cos\theta^*$, the dijet invariant mass, $M^{\rm jj}$, and the fraction of the photon momentum participating in the production of the two jets with highest $E_T^{\rm jet}$, $x_\gamma^{\rm obs}$, are also presented. These variables are sensitive to the dynamics of the underlying dominant subprocesses.

2 Data selection and jet search

The data were collected during the running period 1998-2000, when HERA operated with protons of energy $E_p = 920$ GeV and electrons or positrons of energy $E_e = 27.5$ GeV, and correspond to an integrated luminosity of 82.2 ± 1.9 pb^{-1}. A detailed description of the ZEUS detector can be found elsewhere [9, 10]. A brief outline of the components that are most relevant for this analysis is given below.

Charged particles are tracked in the central tracking detector (CTD) [11], which operates in a magnetic field of 1.43 T provided by a thin superconducting solenoid. The CTD consists of 72 cylindrical drift-chamber layers, organized in nine superlayers covering the

polar-angle[1] region $15^\circ < \theta < 164^\circ$. The transverse-momentum resolution for full-length tracks can be parameterised as $\sigma(p_T)/p_T = 0.0058p_T \oplus 0.0065 \oplus 0.0014/p_T$, with p_T in GeV. The tracking system was used to measure the interaction vertex with a typical resolution along (transverse to) the beam direction of 0.4 (0.1) cm and to cross-check the energy scale of the calorimeter.

The high-resolution uranium–scintillator calorimeter (CAL) [12] covers 99.7% of the total solid angle and consists of three parts: the forward (FCAL), the barrel (BCAL) and the rear (RCAL) calorimeters. Each part is subdivided transversely into towers and longitudinally into one electromagnetic section (EMC) and either one (in RCAL) or two (in BCAL and FCAL) hadronic sections (HAC). The smallest subdivision of the calorimeter is called a cell. Under test-beam conditions, the CAL single-particle relative energy resolutions were $\sigma(E)/E = 0.18/\sqrt{E\,(\mathrm{GeV})}$ for electrons and $\sigma(E)/E = 0.35/\sqrt{E\,(\mathrm{GeV})}$ for hadrons.

The luminosity was measured from the rate of the bremsstrahlung process $e^+p \to e^+\gamma p$. The resulting small-angle energetic photons were measured by the luminosity monitor [13], a lead-scintillator calorimeter placed in the HERA tunnel at $Z = -107$ m.

A three-level trigger system was used to select events online [10, 14]. At the third level, a jet algorithm was applied to the CAL cells and jets were reconstructed using the energies and positions of these cells. Events with at least either one jet with $E_T > 10$ GeV and $\eta < 2.5$ or two jets with $E_T > 6$ GeV and $\eta < 2.5$ were accepted.

Events from collisions between protons and quasi-real photons were selected offline using similar criteria as reported in a previous publication [15].

The longitudinally invariant k_T-cluster algorithm [16] was used in the inclusive mode [17] to reconstruct jets in the hadronic final state. The axis of the jet was defined according to the Snowmass convention [18], where η^{jet} (φ^{jet}) is the transverse energy-weighted mean pseudorapidity (azimuth) of all the particles belonging to that jet. The jets were reconstructed using the CAL and were corrected for detector effects to yield jets of hadrons [15]. Events with at least either one jet of $E_T^{\mathrm{jet}} > 17$ GeV and $-1 < \eta^{\mathrm{jet}} < 2.5$ or two jets of $E_T^{\mathrm{jet1}} > 17$ GeV, $E_T^{\mathrm{jet2}} > 14$ GeV and $-1 < \eta^{\mathrm{jet}} < 2.5$ were retained.

Deep inelastic e^+p scattering neutral current events were removed from the sample by identifying the scattered positron candidate [19] using the pattern of energy distribution in the CAL [20]. The selected sample consisted of events from e^+p interactions with $Q^2 < 1$ GeV^2 and a median of $Q^2 \approx 10^{-3}$ GeV^2. The γp centre-of-mass energy was calculated using the expression $W_{\gamma p} = \sqrt{ys}$, where s is the squared e^+p centre-of-mass

[1] The ZEUS coordinate system is a right-handed Cartesian system, with the Z axis pointing in the proton beam direction, referred to as the "forward direction", and the X axis pointing left towards the centre of HERA. The coordinate origin is at the nominal interaction point.

energy. The inelasticity variable y was reconstructed following the method of Jacquet-Blondel [21] from the energies measured in the CAL cells. The event sample was restricted to the kinematic range $142 < W_{\gamma p} < 293$ GeV.

3 Jet shape and subjet multiplicity definitions

The integrated jet shape, $\psi(r)$, is defined as the fraction of the jet transverse energy that lies inside a cone in the $\eta - \varphi$ plane of radius r concentric with the jet axis [6]:

$$\psi(r) = \frac{E_T(r)}{E_T^{\text{jet}}},$$

where $E_T(r)$ is the transverse energy within the given cone of radius r.

Subjets were resolved within a jet by considering all particles that were associated with it and by repeating the application of the k_T-cluster algorithm, until for every pair of particles i and j the quantity $d_{ij} = \min(E_{T,i}, E_{T,j})^2 \cdot ((\eta_i - \eta_j)^2 + (\varphi_i - \varphi_j)^2)$, where $E_{T,i}$, η_i and φ_i are the transverse energy, pseudorapidity and azimuth of particle i, respectively, was above $d_{cut} = y_{\text{cut}}(E_T^{\text{jet}})^2$. All remaining clusters were called subjets. The subjet multiplicity, n_{subjet}, depends upon the value chosen for the resolution parameter y_{cut}.

4 Monte Carlo simulation

The programs PYTHIA 6.1 [22] and HERWIG 5.9 [23] were used to generate photoproduction events for resolved and direct processes. In PYTHIA, the positron-photon vertex is modelled according to the Weizsäcker-Williams approximation. In the case of HERWIG, the exact matrix elements are used for direct processes ($e^+g \to e^+q\bar{q}$ and $e^+q \to e^+qg$) and the equivalent photon approximation for resolved processes. Events were generated using GRV-HO [24] for the photon parton distributions and CTEQ4M [25] for the proton parton distributions. In both generators, the partonic processes are simulated using LO matrix elements, with the inclusion of initial- and final-state parton showers. In PYTHIA, colour coherence effects are implemented as a restriction on the opening angle of the radiation. The parton-shower algorithm in HERWIG automatically includes angular ordering and azimuthal correlations due to coherence and gluon polarisation. Fragmentation into hadrons is performed using the Lund string model [26] as implemented in JETSET [27] in the case of PYTHIA, and a cluster model [28] in the case of HERWIG. These programs give a very good detailed description of the hadronic final states in e^+e^- annihilation up to the highest energies studied so far [29]. Samples of PYTHIA including multiparton

interactions (MI) [30] with a minimum transverse momentum for the secondary scatter of 1 GeV [3] were used to study the effects of a possible "underlying event".

All generated events were passed through the ZEUS detector- and trigger-simulation programs based on GEANT 3.13 [31]. They were reconstructed and analysed by the same program chain as the data. The jet search was performed using the energy measured in the CAL cells in the same way as for the data. The same jet algorithm was also applied to the final-state particles; the jets found in this way are referred to as hadronic jets.

5 Selection of quark- and gluon-initiated jets

The jet shape at $r = 0.3$, $\psi(r = 0.3)$, and the subjet multiplicity at $y_{\rm cut} = 0.0005$, $n_{\rm subjet}(y_{\rm cut} = 0.0005)$, were used to select quark- and gluon-initiated jets. The different behaviour of these distributions for gluon- and quark-initiated jets was observed previously [4] and is shown in Fig 1. These observables were used to classify the jets according to:

- a gluon-enriched sample ("thick" jets) was defined as those jets with $\psi(r = 0.3) < 0.6$ and $n_{\rm subjet}(y_{\rm cut} = 0.0005) \geq 6$, and
- a quark-enriched sample ("thin" jets) was defined as those jets with $\psi(r = 0.3) > 0.8$ and $n_{\rm subjet}(y_{\rm cut} = 0.0005) < 4$.

Non-overlapping ranges were chosen to suppress migration effects. The values for the cuts in $\psi(r = 0.3)$ and $n_{\rm subjet}(y_{\rm cut} = 0.0005)$ chosen were a compromise between high-purity and large-statistics samples. From the Monte Carlo calculations of PYTHIA (HERWIG), the purity of gluon-initiated jets in the "thick"-jet sample is 67(61)%; the gluon-initiated jets in this sample come mainly from the $qg \to qg$ process. The purity of quark-initiated jets in the "thin"-jet sample is 98(99)%; the quark-initiated jets in the "thin"-jet sample come mainly from the $\gamma g \to q\bar{q}$ process.

After applying the gluon and quark selection cuts, there remain 58264 (11163) jets in the "thick (thin)" inclusive jet data sample and 7297, 356 and 2899 events in the "thick-thick", "thin-thin" and "thick-thin" dijet data samples, respectively.

In the next sections, measurements of cross sections are presented for samples of jets separated according to their shape and subjet multiplicity. The combination of these two methods of separation provides a very powerful tool to separate the subprocesses and observables which probe different aspects of the pQCD calculations are obtained.

6 Inclusive jet cross sections

Using the selected data sample of inclusive jet events, differential inclusive jet cross sections were measured in the kinematic region defined by $Q^2 < 1$ GeV^2 and $142 < W_{\gamma p} < 293$ GeV. These cross sections refer to jets of hadrons with $E_T^{\rm jet} > 17$ GeV and $-1 < \eta^{\rm jet} < 2.5$.

6.1 Measurements of $d\sigma/d\eta^{\rm jet}$

The cross section $d\sigma/d\eta^{\rm jet}$ was measured in the range $-1 < \eta^{\rm jet} < 2.5$ and is presented in Fig. 2 for samples of "thick" and "thin" jets, separated according to the method explained in Section 5. The measured cross sections for the two samples of jets exhibit different behaviours: the $\eta^{\rm jet}$ distribution for "thick" jets peaks at $\eta^{\rm jet} \approx 2$ whereas the distribution for "thin" jets peaks at $\eta^{\rm jet} \approx 0.7$.

Leading-logarithm parton-shower Monte Carlo calculations using PYTHIA, HERWIG and PYTHIA MI for resolved- plus direct-photon processes are compared to the measurements in Fig. 2. The same selection method has been applied to the jets of hadrons in the Monte Carlo event samples and the calculations have been normalised to the total measured cross section of each type. The Monte Carlo predictions provide a good description of the shape of the "thin"-jet data distribution. The shape of the "thick"-jet data distribution is reasonably well described by PYTHIA or PYTHIA MI, but the prediction of HERWIG fails to describe this data distribution. From the calculation of PYTHIA (HERWIG), the sample of "thick" jets is predicted to contain 16(13)% of gg subprocesses in the final state and 52(48)% of gq, and a contamination from processes with only quarks in the final state of 33(39)%. There is a large contribution from gq final states in the "thick"-jet sample because the partonic cross section for the resolved subprocess $qg \to qg$ is much larger than the cross section for the subprocesses $q\bar{q} \to gg$ plus $gg \to gg$. The sample of "thin" jets contains 65(64)% of qq subprocesses and 33(34)% of qg, with a contamination of 2(1)% from gg subprocesses.

6.2 Measurements of $d\sigma/dE_T^{\rm jet}$

The cross section $d\sigma/dE_T^{\rm jet}$ was measured in the range $17 < E_T^{\rm jet} < 71$ GeV and is presented in Fig. 3 for samples of "thick" and "thin" jets, separated according to the method explained in Section 5. The measured cross section for the "thin"-jet sample exhibits a harder spectrum than that for the "thick"-jet sample.

The Monte Carlo calculations using PYTHIA, HERWIG and PYTHIA MI are compared to the measurements in Fig. 3 and have been obtained using the same selection method as

for the data. The calculations have been normalised to the total measured cross section of each type. The Monte Carlo predictions provide a good description of the shape of the "thin"-jet data distribution. The shape of the "thick"-jet data distribution is reasonably well described by PYTHIA or HERWIG, but the prediction of PYTHIA MI fails to describe the high $E_T^{\rm jet}$ tail.

7 Dijet cross sections

Using the selected data sample of dijet events, differential dijet cross sections were measured in the kinematic region defined by $Q^2 < 1$ GeV^2 and $142 < W_{\gamma p} < 293$ GeV. These cross sections refer to the two highest-$E_T^{\rm jet}$ jets of hadrons in the event with $E_T^{\rm jet1} > 17$ GeV, $E_T^{\rm jet2} > 14$ GeV and $-1 < \eta^{\rm jet} < 2.5$.

7.1 Measurements of $d\sigma/d\cos\theta^*$

For samples of "thick-thick" or "thin-thin" jets, only the absolute value of $\cos\theta^*$ can be determined because the outgoing jets are indistinguishable. The differential dijet cross section as a function of $|\cos\theta^*|$ has been measured in the range $|\cos\theta^*| < 0.8$ for dijet invariant masses $M^{\rm jj} > 52$ GeV. The region of phase space in the $(M^{\rm jj}, |\cos\theta^*|)$ plane was chosen in order to minimise the biases introduced by selecting jets with $E_T^{\rm jet1} > 17$ GeV and $E_T^{\rm jet2} > 14$ GeV. The measured $d\sigma/d|\cos\theta^*|$ for the samples of "thick-thick" jet events and "thin-thin" jet events are presented in Fig. 4. The measured and predicted cross sections were normalised so as to have a value of unity at $|\cos\theta^*| = 0.1$. The $|\cos\theta^*|$ distribution for the "thick-thick" jet sample increases as $|\cos\theta^*|$ increases, whereas for the "thin-thin" jet sample is approximately constant within the measured range. The increase at $|\cos\theta^*| = 0.7$ with respect to the value at $|\cos\theta^*| = 0.1$ for "thick-thick" jet events is seven times larger than the increase for "thin-thin" jet events.

Calculations from PYTHIA, HERWIG and PYTHIA MI for "thick-thick" jet events and "thin-thin" jet events are compared to the data in Fig. 4. The predictions from PYTHIA give the best description of the shape of the measured $d\sigma/d|\cos\theta^*|$. In this case, PYTHIA (HERWIG) predicts 19(14)% of gg-final-state subprocesses, 52(50)% of gq and 29(36)% of qq for the "thick-thick" jet sample in the kinematic region of this measurement. For the "thin-thin" jet sample, the predictions are: 81.2(80.8)% of qq subprocesses, 18.3(19.1)% of qg and 0.5(0.1)% of gg. The differences observed in the measured $d\sigma/d|\cos\theta^*|$ for the two samples are adequately reproduced by the calculations and understood in terms of the dominant two-body processes: the resolved subprocess $qg \to qg$ for the "thick-thick"-jet sample and the direct subprocess $\gamma g \to q\bar{q}$ for the "thin-thin" jet sample.

The sample of dijet events with one "thick" jet and one "thin" jet allows a measurement of the unfolded $d\sigma/d\cos\theta^*_{\rm thick}$ cross section, since in this case the two jets can be distinguished. Fig. 5 shows the measured dijet cross section as a function of $\cos\theta^*_{\rm thick}$. The measured and predicted cross sections were normalised so as to have a value of unity at $\cos\theta^*_{\rm thick} = 0.1$. The dijet angular distribution was measured with respect to the "thick" jet and shows a different behaviour on the negative and positive sides: the measured cross section at $\cos\theta^*_{\rm thick} = 0.7$ is approximately two times larger than the one at $\cos\theta^*_{\rm thick} = -0.7$. The calculations from PYTHIA and HERWIG give a good description of the shape of the measured $d\sigma/d\cos\theta^*_{\rm thick}$. The predictions of PYTHIA (HERWIG) for the partonic content are: 56(41)% of qg subprocesses, 3(6)% of gg and 41(53)% of qq. The observed asymmetry is adequately reproduced by the calculation and is understood in terms of the dominant resolved subprocess $q_\gamma g_p \to qg$. The $\cos\theta^*_{\rm thick}$ distribution for this subprocess is asymmetric due to the different dominant diagrams in the regions $\cos\theta^*_{\rm thick} \to \pm 1$: t-channel gluon exchange ($\cos\theta^*_{\rm thick} \to +1$) and u-channel quark exchange ($\cos\theta^*_{\rm thick} \to -1$).

7.2 Measurements of $d\sigma/dM^{\rm jj}$ and $d\sigma/dx_\gamma^{\rm obs}$

The differential dijet cross section as a function of $M^{\rm jj}$ has been measured in the range $52 < M^{\rm jj} < 123$ GeV for $|\cos\theta^*| < 0.8$. The measured $d\sigma/dM^{\rm jj}$ for the samples of "thick-thick" jet events and "thin-thin" jet events are presented in Fig. 6. The measured $d\sigma/dM^{\rm jj}$ cross sections decrease as $M^{\rm jj}$ increases, but the measured distribution for the "thin-thin" jet sample exhibits a harder spectrum, as was seen for the inclusive jet cross section as a function of $E_T^{\rm jet}$.

The Monte Carlo calculations from PYTHIA, HERWIG and PYTHIA MI are compared to the data in Fig. 6 and give a good description of the shape of the measured $d\sigma/dM^{\rm jj}$.

The different shape in both cross sections is understood in terms of the dominant two-body processes: the "thick-thick" jet sample is dominated by the resolved subprocess $qg \to qg$ and the "thin-thin" jet sample is dominated by the direct subprocess $\gamma g \to q\bar{q}$. Resolved and direct processes can be separated by using the $x_\gamma^{\rm obs}$ variable which is defined as

$$x_\gamma^{\rm obs} = \frac{1}{2yE_e}(E_T^{\rm jet1}e^{-\eta^{\rm jet1}} + E_T^{\rm jet2}e^{-\eta^{\rm jet2}}). \qquad (1)$$

Resolved and direct processes populate different regions in $x_\gamma^{\rm obs}$, with the direct processes concentrated at high values of $x_\gamma^{\rm obs}$. The variable $x_\gamma^{\rm obs}$ was reconstructed via the above formula using the calorimetric-jet transverse energies and $y_{cal} = W^2_{\rm cal}/s$, since many systematic uncertainties in the measurement of energy by the CAL cancel out event by event in the ratio of Eq. (1). The dijet cross section as a function of $x_\gamma^{\rm obs}$ is presented in Fig. 7

and is reasonably well described by the Monte Carlo predictions of PYTHIA and HERWIG; the description provided by PYTHIA MI is slightly worse. The cross section for the "thick-thick" jet sample is approximately constant as a function of $x_\gamma^{\rm obs}$ whereas the cross section for the "thin-thin" jet sample peaks at high $x_\gamma^{\rm obs}$ values.

The measured dijet cross sections as functions of $M^{\rm jj}$ and $x_\gamma^{\rm obs}$ are shown in Fig. 8 for samples of events with "thick-thick", "thin-thin" and "thick-thin" jets. The "thick-thin" sample is a mixture of the $qg \to qg$ and $\gamma g \to q\bar{q}$ subprocesses and shows the expected intermediate behaviour between the "thick-thick" and "thin-thin" jet samples.

8 Summary and conclusions

Measurements of differential inclusive jet and dijet cross sections in the photoproduction regime in ep collisions at a centre-of-mass energy of 318 GeV using the data collected by ZEUS in 1998 to 2000, corresponding to an integrated luminosity of 82.2 pb^{-1}, have been presented. The measurements refer to jets identified with the longitudinally invariant k_T-cluster algorithm in the inclusive mode and selected according to $E_T^{\rm jet1} > 17$ GeV, $E_T^{\rm jet2} > 14$ GeV and $-1 < \eta^{\rm jet} < 2.5$ and given in the kinematic region defined by $Q^2 < 1$ GeV^2 and $142 < W_{\gamma p} < 293$ GeV. Leading-logarithm parton shower Monte Carlo models give a good description of the data. The internal structure of the jets, in terms of the integrated jet shape and subjet multiplicity, has been used to select samples enriched in quark- ("thin") and gluon-initiated ("thick") jets.

The inclusive jet cross sections $d\sigma/d\eta^{\rm jet}$ and $d\sigma/dE_T^{\rm jet}$ have been measured in the range $-1 < \eta^{\rm jet} < 2.5$ integrated over $E_T^{\rm jet} > 17$ GeV for "thick" and "thin" jet samples. The measurements show the expected behaviour for samples enriched in gluon- and quark-initiated jets, respectively.

The dijet cross section as a function of $\cos\theta^*$ has been measured in the range $|\cos\theta^*| < 0.8$ integrated over $M^{\rm jj} > 52$ GeV. The $|\cos\theta^*|$ distribution for the "thick-thick" jet sample displays a similar behaviour to the one expected for a sample enriched in processes mediated by gluon exchange, whereas that for the "thin-thin" jet sample shows a behaviour similar to a sample enriched in processes mediated by quark exchange. The dijet cross section $d\sigma/d\cos\theta^*_{\rm thick}$ has been measured in the region $-0.8 < \cos\theta^*_{\rm thick} < 0.8$ integrated over $M^{\rm jj} > 52$ GeV for a sample of events with "thick-thin" jets. The measured cross section $d\sigma/d\cos\theta^*_{\rm thick}$ exhibits a large asymmetry, which is consistent with the expected dominance of gluon (quark) exchange as $\cos\theta^*_{\rm thick} \to +1$ ($\cos\theta^*_{\rm thick} \to -1$).

The dijet cross section as a function of $M^{\rm jj}$ and $x_\gamma^{\rm obs}$ has been measured for samples of events with "thick-thick" or "thin-thin" jets. The cross section for the sample of "thick-thick" jets shows a behaviour consistent with the dominance of the resolved $qg \to qg$

subprocess whereas the sample with "thin-thin" jets is consistent with the dominance of the direct $\gamma g \to q\bar{q}$ subprocess.

Acknowledgements

We thank the DESY Directorate for their strong support and encouragement. The remarkable achievements of the HERA machine group were essential for the successful completion of this work and are greatly appreciated.

References

[1] C.H. Llewellyn Smith, Phys. Lett. **B 79**, 83 (1978);
I. Kang and C.H. Llewellyn Smith, Nucl. Phys. **B 166**, 413 (1980);
J.F. Owens, Phys. Rev. **D 21**, 54 (1980);
M. Fontannaz, A. Mantrach and D. Schiff, Z. Phys. **C 6**, 241 (1980).

[2] W.J. Stirling and Z. Kunszt, *Proc. HERA Workshop*, R.D. Peccei (ed.), Vol. 2, p. 331. DESY, Hamburg, Germany (1987);
M. Drees and F. Halzen, Phys. Rev. Lett. **61**, 275 (1988);
M. Drees and R.M. Godbole, Phys. Rev. Lett. **61**, 682 (1988);
M. Drees and R.M. Godbole, Phys. Rev. **D 39**, 169 (1989);
H. Baer, J. Ohnemus and J.F. Owens, Z. Phys. **C 42**, 657 (1989);
H. Baer, J. Ohnemus and J.F. Owens, Phys. Rev. **D 40**, 2844 (1989).

[3] ZEUS Coll., J. Breitweg et al., Eur. Phys. J. **C 2**, 61 (1998).

[4] ZEUS Coll., *Substructure Dependence of Dijet Cross Sections in Photoproduction at HERA*. Abstract 906, XXXth International Conference on High Energy Physics, Osaka, Japan, 2000.

[5] ZEUS Coll., M. Derrick et al., Phys. Lett. **B 384**, 401 (1996).

[6] S.D. Ellis, Z. Kunszt, D.E. Soper, Phys. Rev. Lett. **69**, 3615 (1992).

[7] S. Catani et al., Nucl. Phys. **B 377**, 445 (1992);
S. Catani et al., Nucl. Phys. **B 383**, 419 (1992);
M.H. Seymour, Nucl. Phys. **B 421**, 545 (1994);
M.H. Seymour, Phys. Lett. **B 378**, 279 (1996).

[8] ZEUS Coll., *Measurements of Jet Substructure in Photoproduction at HERA*. Abstract 530, International Europhysics Conference on High Energy Physics, Tampere, Finland, 1999.

[9] ZEUS Coll., M. Derrick et al., Phys. Lett. **B 293**, 465 (1992).

[10] ZEUS Coll., U. Holm (ed.), *The ZEUS Detector*. Status Report (unpublished), DESY (1993), available on `http://www-zeus.desy.de/bluebook/bluebook.html`.

[11] N. Harnew et al., Nucl. Inst. Meth. **A 279**, 290 (1989);
B. Foster et al., Nucl. Phys. Proc. Suppl. **B 32**, 181 (1993);
B. Foster et al., Nucl. Inst. Meth. **A 338**, 254 (1994).

[12] M. Derrick et al., Nucl. Inst. Meth. **A 309**, 77 (1991);
A. Andresen et al., Nucl. Inst. Meth. **A 309**, 101 (1991);
A. Caldwell et al., Nucl. Inst. Meth. **A 321**, 356 (1992);
A. Bernstein et al., Nucl. Inst. Meth. **A 336**, 23 (1993).

[13] J. Andruszków et al., Preprint DESY-92-066, DESY, 1992;
ZEUS Coll., M. Derrick et al., Z. Phys. **C 63**, 391 (1994);
J. Andruszków et al., Acta Phys. Pol. **B 32**, 2025 (2001).

[14] W. H. Smith, K. Tokushuku and L. W. Wiggers, *Proc. Computing in High-Energy Physics (CHEP), Annecy, France, Sept. 1992*, C. Verkerk and W. Wojcik (eds.), p. 222. CERN, Geneva, Switzerland (1992). Also in preprint DESY 92-150B.

[15] ZEUS Coll., S. Chekanov et al., Phys. Lett. **B 560**, 7 (2003).

[16] S. Catani et al., Nucl. Phys. **B 406**, 187 (1993).

[17] S.D. Ellis and D.E. Soper, Phys. Rev. **D 48**, 3160 (1993).

[18] J.E. Huth et al., *Research Directions for the Decade. Proceedings of Summer Study on High Energy Physics, 1990*, E.L. Berger (ed.), p. 134. World Scientific (1992). Also in preprint FERMILAB-CONF-90-249-E.

[19] H. Abramowicz, A. Caldwell and R. Sinkus, Nucl. Inst. Meth. **A 365**, 508 (1995);
R. Sinkus and T. Voss, Nucl. Inst. Meth. **A 391**, 360 (1997).

[20] ZEUS Coll., M. Derrick et al., Phys. Lett. **B 322**, 287 (1994).

[21] F. Jacquet and A. Blondel, *Proceedings of the Study for an ep Facility for Europe*, U. Amaldi (ed.), p. 391. Hamburg, Germany (1979). Also in preprint DESY 79/48.

[22] T. Sjöstrand, Comp. Phys. Comm. **82**, 74 (1994).

[23] G. Marchesini et al., Comp. Phys. Comm. **67**, 465 (1992).

[24] M. Glück, E. Reya and A. Vogt, Phys. Rev. **D 45**, 3986 (1992);
M. Glück, E. Reya and A. Vogt, Phys. Rev. **D 46**, 1973 (1992).

[25] H.L. Lai et al., Phys. Rev. **D 55**, 1280 (1997).

[26] B. Andersson et al., Phys. Rep. **97**, 31 (1983).

[27] T. Sjöstrand, Comp. Phys. Comm. **39**, 347 (1986);
T. Sjöstrand and M. Bengtsson, Comp. Phys. Comm. **43**, 367 (1987).

[28] B.R. Webber, Nucl. Phys. **B 238**, 492 (1984).

[29] See e.g. ALEPH Coll., R. Barate et al., Phys. Rep. **294**, 1 (1998).

[30] T. Sjöstrand and M. van Zijl, Phys. Rev. **D 36**, 2019 (1987).

[31] R. Brun et al., GEANT3, Technical Report CERN-DD/EE/84-1, CERN, 1987.

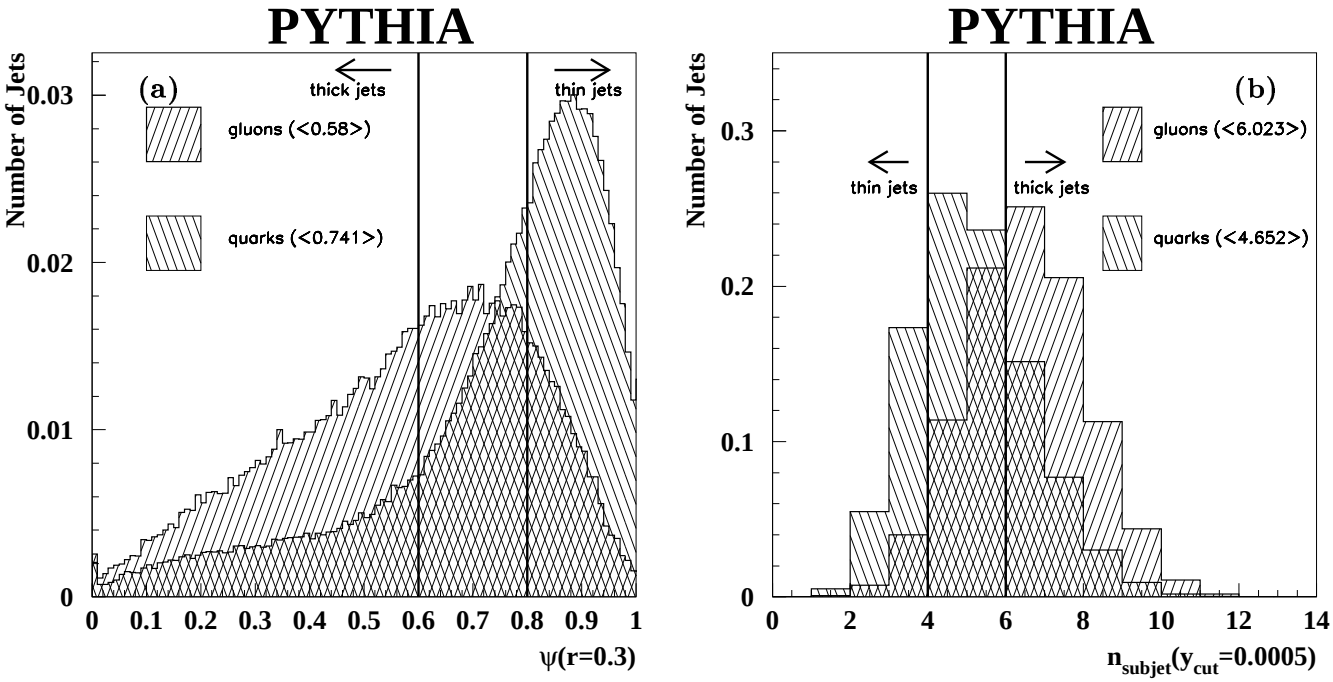

Figure 1: *The predicted integrated jet shape distribution $\psi(r)$ at $r = 0.3$ (a) and the predicted subjet multiplicity distribution $n_{\rm subjet}$ at $y_{\rm cut} = 0.0005$ (b) at the hadron level for samples of gluon- and quark-initiated jets simulated using the program PYTHIA.*

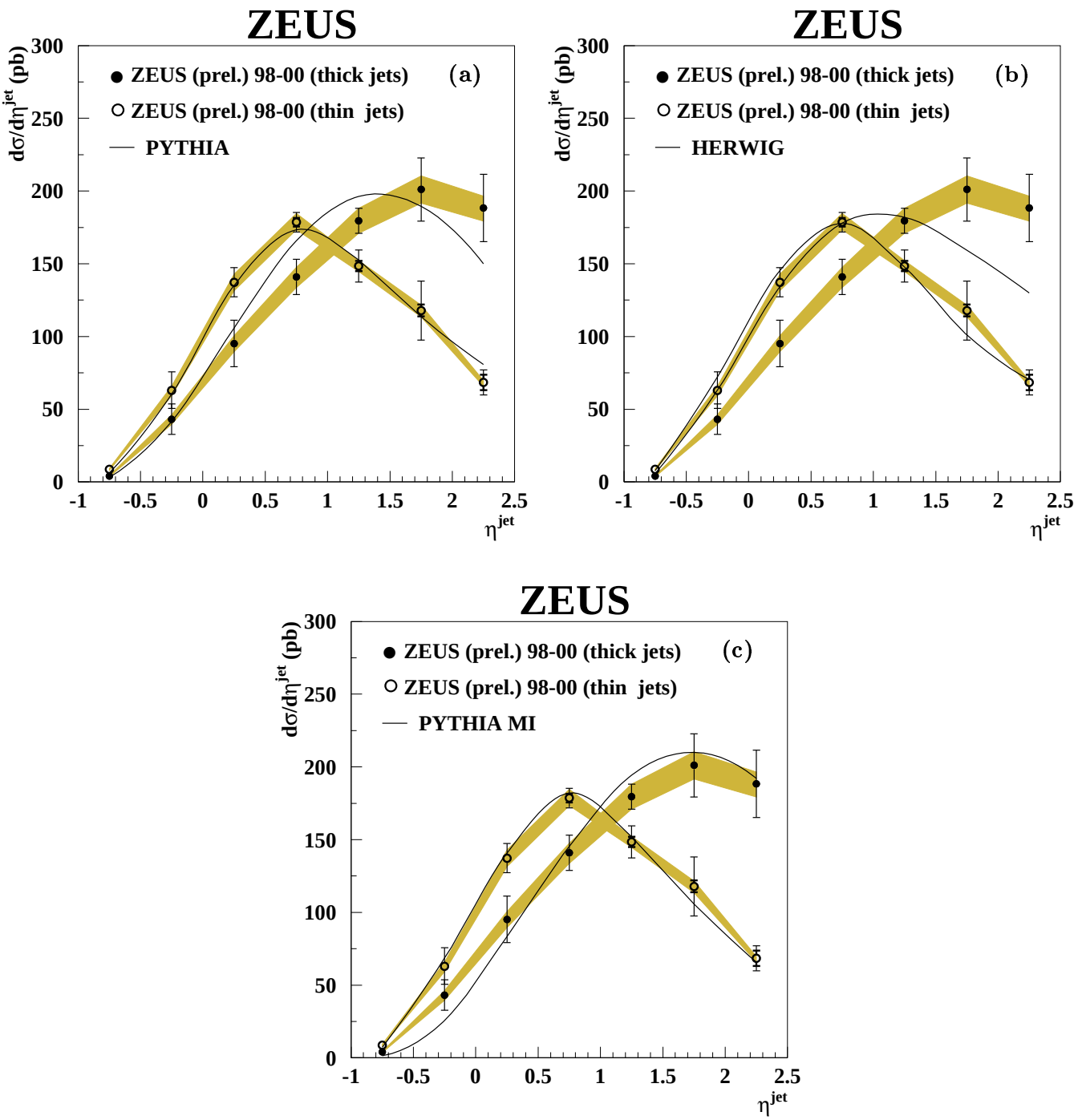

Figure 2: *Differential ep cross section $d\sigma/d\eta^{\rm jet}$ for inclusive jet production integrated over $E_T^{\rm jet} > 17$ GeV in the kinematic region defined by $Q^2 < 1$ GeV^2 and $142 < W_{\gamma p} < 293$ GeV. The jets have been selected according to their shape and subjet multiplicity (see text) in "thick" (black dots) and "thin" (open circles) jets. The thick error bars represent the statistical uncertainties of the data, and the thin error bars show the statistical and systematic uncertainties —not associated with the uncertainty in the absolute energy scale of the jets— added in quadrature. The shaded band displays the uncertainty due to the absolute energy scale of the jets. For comparison, leading-logarithm parton-shower Monte Carlo calculations using PYTHIA (a), HERWIG (b) and PYTHIA MI (c) for resolved- plus direct-photon processes separated according to the same criteria as in the data are included. The Monte Carlo calculations have been normalised to the total measured cross section of each type.*

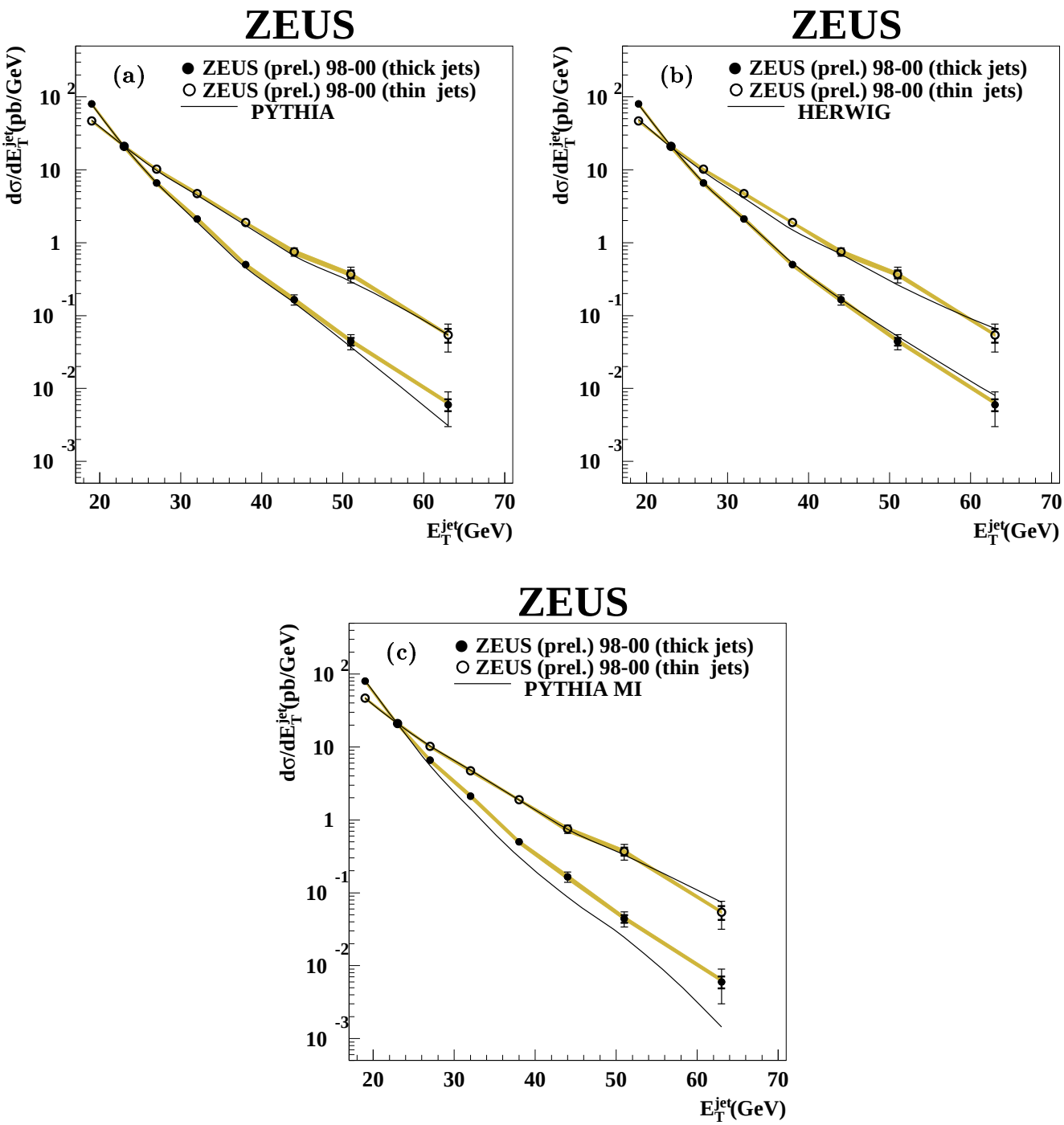

Figure 3: *Differential ep cross section* $d\sigma/dE_T^{\rm jet}$ *for inclusive jet production integrated over* $-1 < \eta^{\rm jet} < 2.5$ *in the kinematic region defined by* $Q^2 < 1$ *GeV*^{2} *and* $142 < W_{\gamma p} < 293$ *GeV. Other details as in the caption to Fig. 2.*

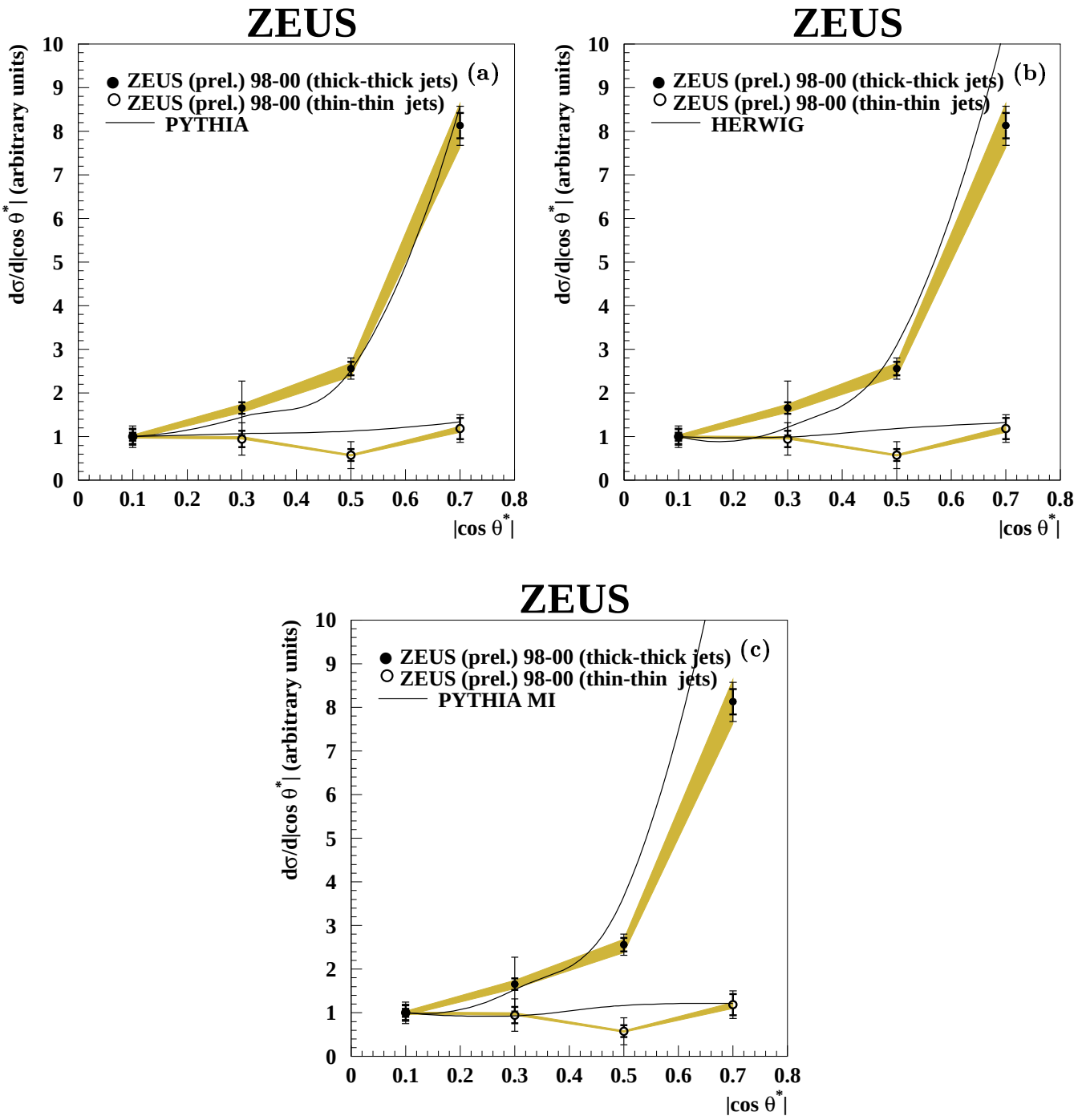

Figure 4: *Differential ep cross section $d\sigma/d|\cos\theta^*|$ for dijet production integrated over $E_T^{\mathrm{jet1}} > 17$ GeV, $E_T^{\mathrm{jet2}} > 14$ GeV and $-1 < \eta^{\mathrm{jet}} < 2.5$ in the kinematic region defined by $Q^2 < 1$ GeV^2, $142 < W_{\gamma p} < 293$ GeV and $M^{\mathrm{jj}} > 52$ GeV. The cross section is for events with "thick-thick" (black dots) and "thin-thin" (open circles) jets selected according to their shape and subjet multiplicity (see text). Other details as in the caption to Fig. 2.*

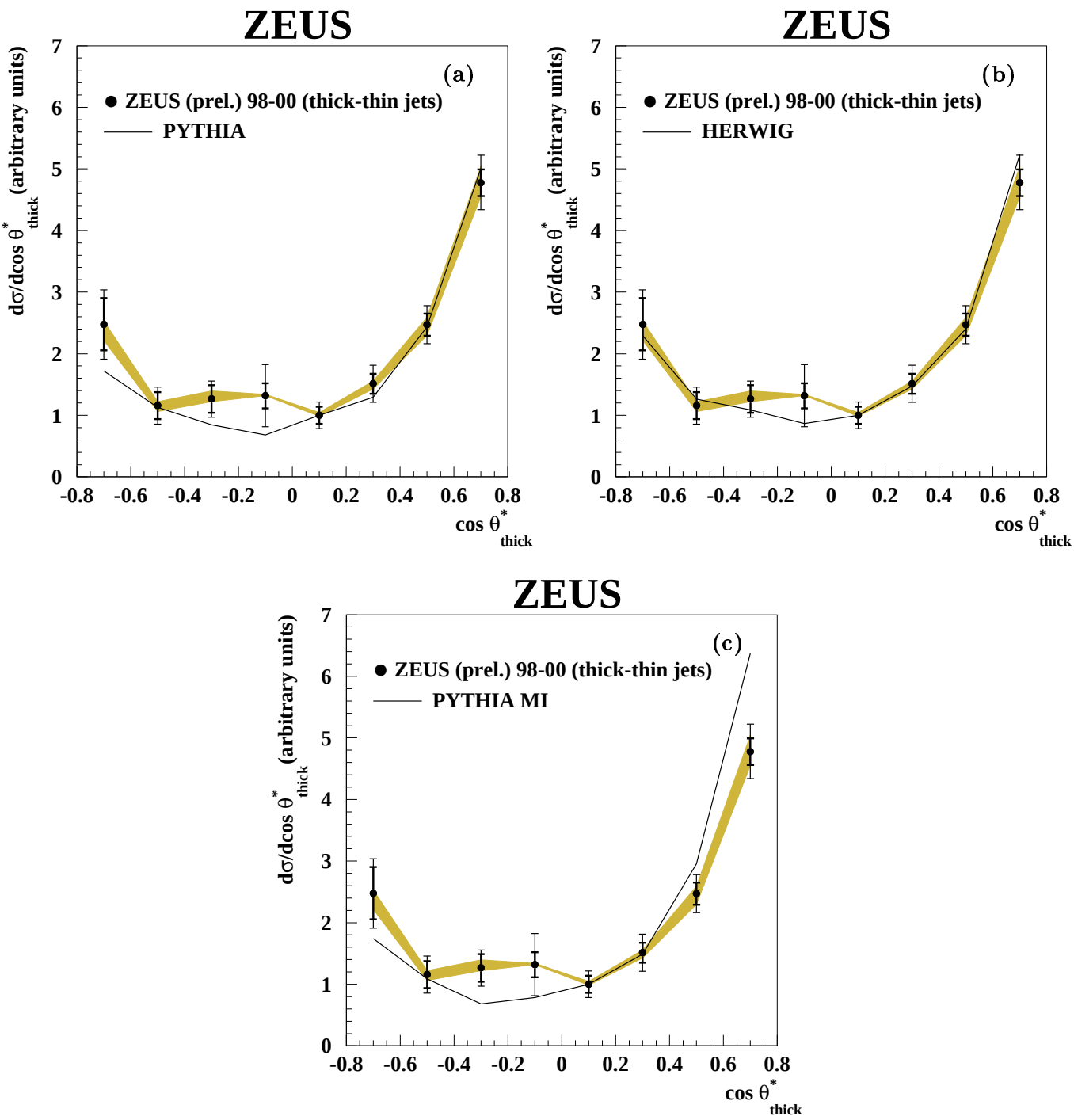

Figure 5: *Differential ep cross section* $d\sigma/d\cos\theta^*_{\rm thick}$ *for dijet production integrated over* $E_T^{\rm jet\,1} > 17$ *GeV,* $E_T^{\rm jet2} > 14$ *GeV and* $-1 < \eta^{\rm jet} < 2.5$ *in the kinematic region defined by* $Q^2 < 1$ *GeV*^{2}, $142 < W_{\gamma p} < 293$ *GeV and* $M^{\rm jj} > 52$ *GeV. The cross section is for dijet events with "thick-thin" jets (black dots) selected according to their shape and subjet multiplicity (see text). Other details as in the caption to Fig. 2.*

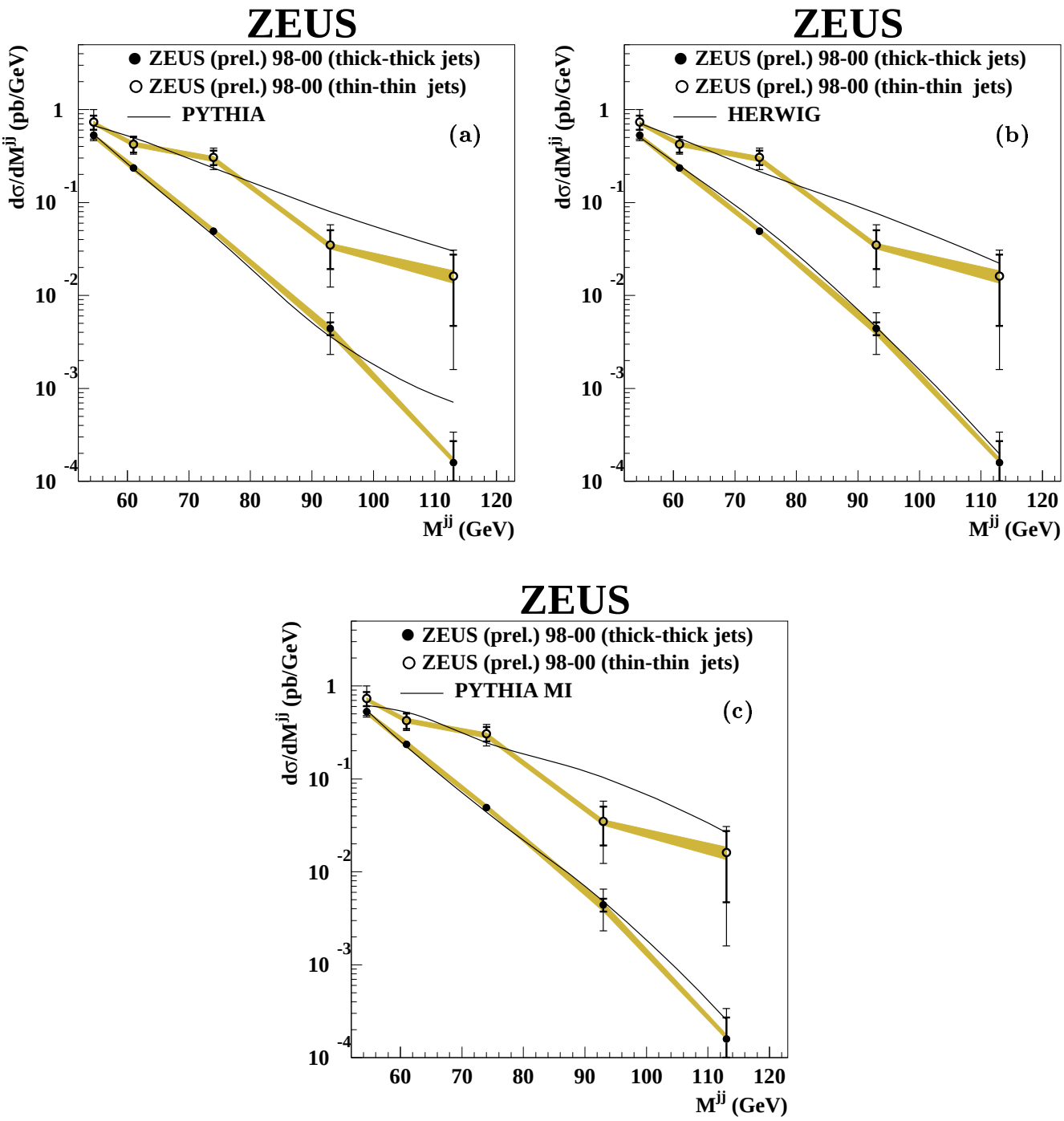

Figure 6: *Differential ep cross section $d\sigma/dM^{jj}$ for dijet production integrated over $E_T^{jet1} > 17$ GeV, $E_T^{jet2} > 14$ GeV and $-1 < \eta^{jet} < 2.5$ in the kinematic region defined by $Q^2 < 1$ GeV^2, $142 < W_{\gamma p} < 293$ GeV and $|\cos\theta^*| < 0.8$. Other details as in the caption to Fig. 4.*

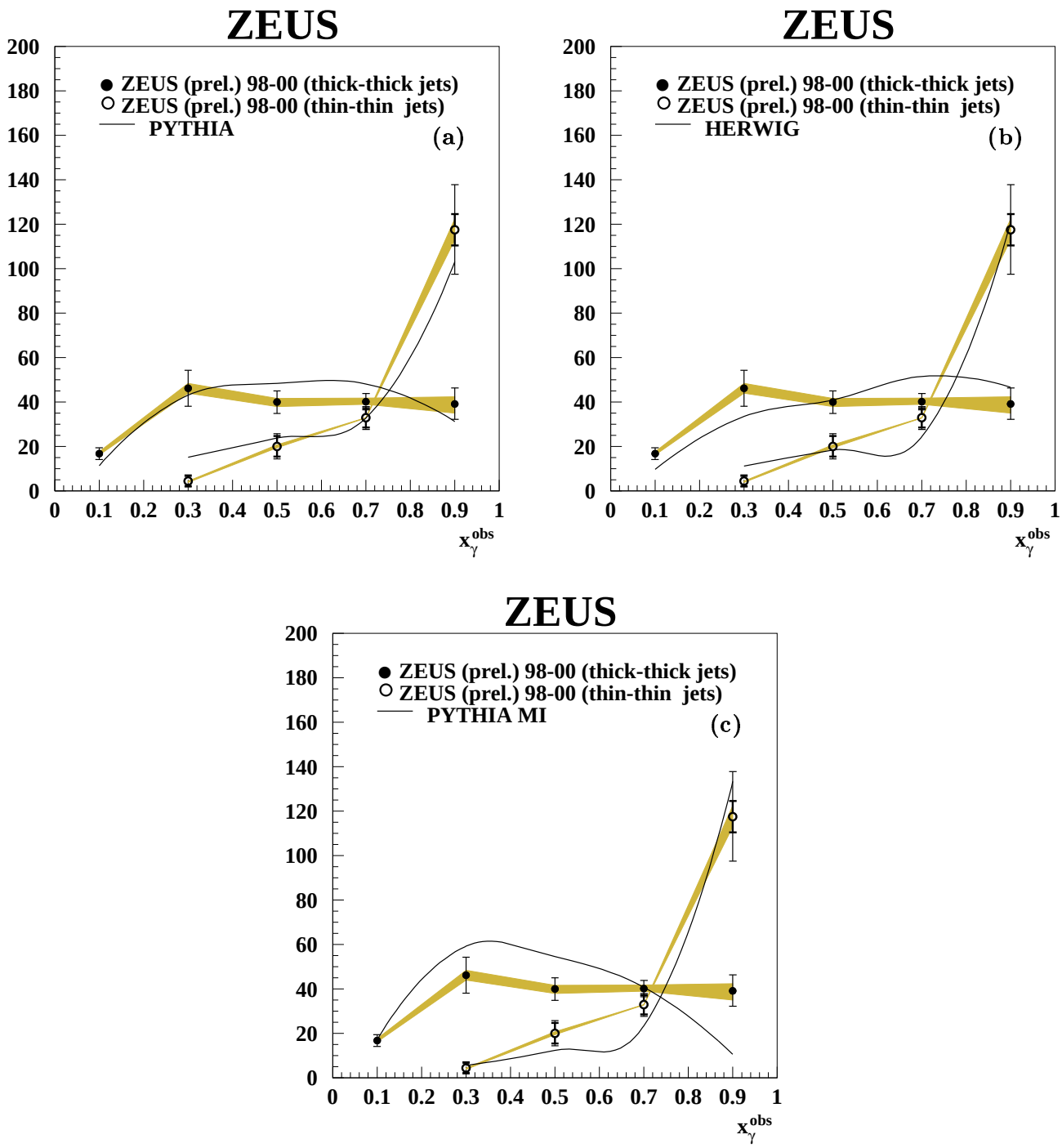

Figure 7: *Differential ep cross section $d\sigma/dx_\gamma^{\rm obs}$ for dijet production integrated over $E_T^{\rm jet\,1} > 17$ GeV, $E_T^{\rm jet2} > 14$ GeV and $-1 < \eta^{\rm jet} < 2.5$ in the kinematic region defined by $Q^2 < 1$ GeV^2 and $142 < W_{\gamma p} < 293$ GeV. Other details as in the caption to Fig. 4.*

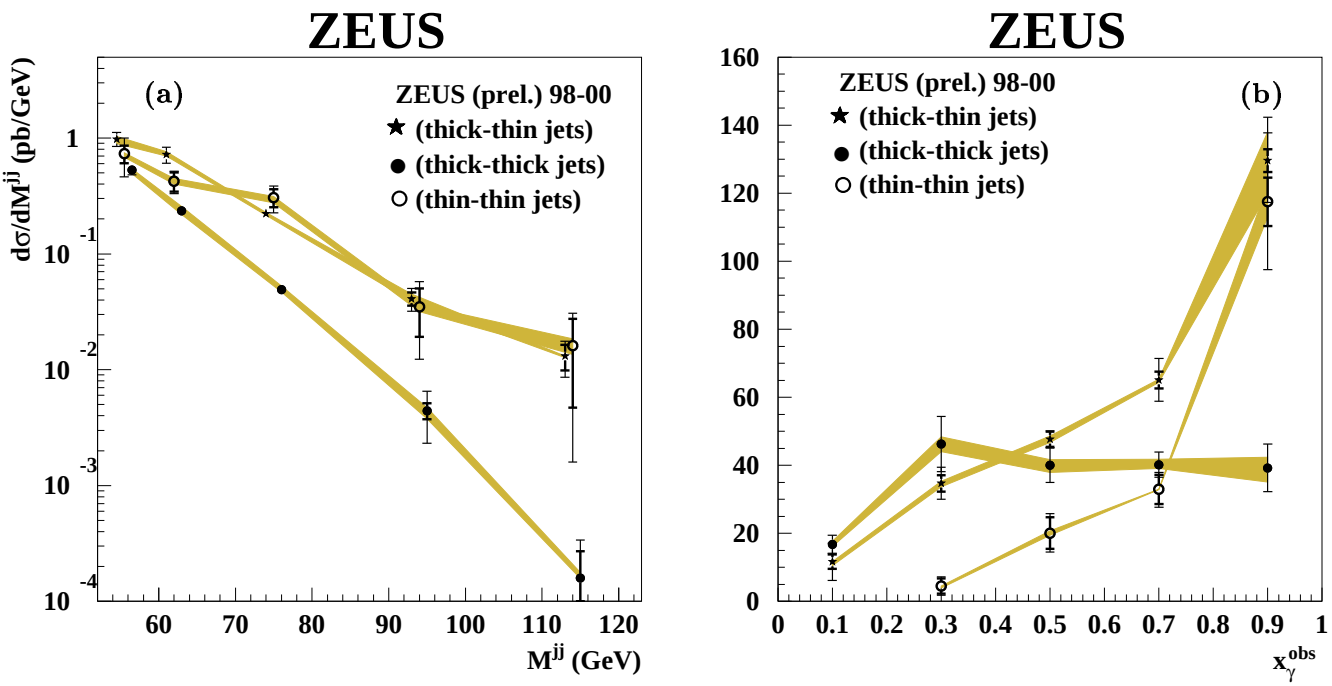

Figure 8: *Differential ep cross sections $d\sigma/dM^{jj}$ (a) and $d\sigma/dx_\gamma^{obs}$ (b) for dijet production integrated over $E_T^{jet1} > 17$ GeV, $E_T^{jet2} > 14$ GeV and $-1 < \eta^{jet} < 2.5$ in the kinematic region defined by $Q^2 < 1$ GeV^2 and $142 < W_{\gamma p} < 293$ GeV for "thick-thick" jets (black dots), "thin-thin" jets (open circles) and "thick-thin" jets (black stars). The data points in (a) have been moved by 1 GeV ("thin-thin" jets) and 2 GeV ("thick-thick" jets) in M^{jj} for a better display. Other details as in the caption to Fig. 4.*